J Inno Sci Eng, 2025, 9(1):103-117

DOI:https://doi.org/ 10.38088/jise.1630283

Research Article

The Effect of Half Wave Pulsed Current Charging on Age and Capacity Fade for Lithium-ion Batteries

Muhammed Reşit ÇORAPSIZ*

Department of Electrical & Electronics Engineering, Erzurum Technical University, Erzurum, TR-25100, Türkiye

ARTICLE INFO

Received Date: 31/01/2025
Accepted Date: 4/05/2025

Cite this paper as:
Çorapsız, M. R. (2025). The effect of half wave pulsed current charging on age and capacity fade for Lithium-ion batteries. *Journal of Innovative Science and Engineering.* 9(1), 103-117.

*Corresponding author: Muhammed Reşit ÇORAPSIZ
E-mail:r.corapsiz@erzurum.edu.tr

Keywords:
Li-ion batteries
Continuous current – Continuous voltage charging (CC-CV)
Pulsed current charge (PPC)
Life cycle
Capacity fade

ABSTRACT

This study proposes a new pulsed charging current technique to reduce aging and capacity losses in lithium-ion battery cells. The charging techniques developed to minimize aging and capacity losses are critical for battery cells with longer life cycles and higher energy efficiency. Continuous Current – Continuous Voltage charging (CC-CV), Positive Pulsed Current (PPC), and proposed Alternating Half Wave Pulsed Current (AHWPC) techniques were tested on a $12.8V - 40Ah$ Li-ion battery. In PPC and AHWPC techniques, the pulse frequency of the charging current is chosen as $f_{i_{ch}} = 1\ Hz$. The average value of the charging current for PPC and AHWPC techniques is calculated based on the CC-CV technique. The aging and capacity losses caused by the three charging techniques in the battery were measured in five different scenarios: at various temperatures, different discharge currents, and different depths of discharge (DoD). Using the AHWPC technique, improvements of 45.93%, 46.57% and 46.29% were achieved in cell aging compared to the CC-CV technique at temperatures of 20°C, 30°C and 40°C, respectively. According to the results, the proposed AHWPC technique performed better than the PPC and CC-CV techniques in all test conditions.

1. Introduction

Due to the increasing need for mobile devices around the world, the demand for high-performance rechargeable batteries is increasing day by day. The market share of Lithium-ion batteries (LIBs) is rapidly growing, expanding their application areas [1]. According to the report published by Precedence Research, the size of the global LIBs market will be worth 70 Billion USD in the 2020s, and this value is expected to exceed 370.05 Billion USD by 2032 [2]. LIBs are considered to be one of the most promising power sources for mobile electronic products, portable power devices, and vehicles [3]. This is because they have advantages such as high energy density, highly efficient charge/discharge rates, and high cycle life. LIBs, which have been preferred especially in vehicle technology in recent years, pose a disadvantage in terms of charging time. This situation causes rapid aging and capacity loss problems in cells if efficient charging techniques are not provided. While chemical research focuses on material design [4,5] engineering studies aim to develop charging techniques that enhance cycle life, efficiency, and capacity retention [6-8]. In general, the expected performance of a battery cell is a short charge time, long discharge time, and sufficiently long service life. It is insufficient that a particular charging technique proposed by the researchers solves only one of these two problems. A commercialized battery cell has a limited charge and discharge current, and these values are provided by the manufacturer. During the charging and discharging processes, the reaction between the negative electrode and the electrolyte produces a passive layer called the solid electrolyte interphase (SEI). The growth of this layer causes the loss of active lithium ions, resulting in capacity loss [9,10] Reducing the capacity loss and extending the service life of a commercialized LIB is only possible with the development of efficient charging techniques. These techniques will prevent capacity loss at certain rates and contribute to the extension of the cycle life of LIBs. In the literature and industry, the Constant Current (CC) - Constant Voltage (CV) technique is a common approach for charging LIBs [11]. However, in a LIB cell charged by the CC-CV technique, the CV phase contributes about a quarter of the discharge capacity and accounts for about half of the charging time. In addition, the cell exposed to continuous charging current heats up more, leading to increased thermal losses. To solve these problems, pulsed charging current techniques have been proposed [12] in different techniques including Positive Pulsed Current (PPC) mode [13], Pulsed Current-Constant Current (PCCC) mode [14], Negative Pulsed Current (NPC) mode [15], Alternating Pulsed Current (APC) mode [14] Sinusoidal Ripple Current (SRC) mode [10] and Alternating Sinusoidal Ripple Current (ASRC) mode [16].

The SRC strategy is proposed to determine the optimal pulsed charging current frequency (fz_{min}) of a LIBs. It is argued that this technique improves the charging time by about 17%, charging efficiency by 1.9%, maximum temperature rise by 45.8%, and cycle life by 16.1% compared to the CC-CV technique [16]. The NPC technique is discussed in [17], which provides the battery cell with higher discharge capacity and longer cycle life by improving active material utilization with short relaxation times and short discharge pulses during charging. As a result of XRD (X-Ray Diffraction) and SEM (Scanning Electron Microscope) studies obtained from this technique, it was observed that pulsed charging maintains the stability of the cathode better than CC-CV and prevents the increase in SEI formation. Since different Li-ion cells were used in most of the studies, the same pulsed current profiles may not provide the same performance for all Li-ion cells. This is because the electrode and electrolyte materials, capacity values, maximum charge (I_{max-ch}) and maximum discharge ($I_{max-disch}$) rates are not the same for different cells. In addition, the maximum discharge currents of the cells are usually much higher than the maximum charge currents. For example, these values are $I_{max-ch} = 1.7A$ and $I_{max-disch} = 10A$ for the MOLICELL INR-18650-35A Li-ion cell while $I_{max-ch} = 2.5A$ and $I_{max-disch} = 20A$ for the ORION INR-18650P cell [18,19]. Therefore, the cycle life and capacity fade for a Li-ion cell are more affected by high charge currents than by high discharge currents [20].

In the literature, pulsed charging currents are widely claimed to increase cycle life and reduce capacity losses, but some studies claim the opposite. In [21], PCCC mode is proposed, and it is asserted that the periodic pulse effect is detrimental to Li-ion battery performance when compared to a constant current profile based on the same average current. There are some reasons why the effects of pulse charging techniques on capacity loss and aging are favorable for some studies and unfavorable for others. Among these reasons, the amplitude, duty cycle, and the frequency of the pulsed charge profile used to charge the battery can be shown. In [7], the cycle life and performance of LIBs were studied by applying the charging current in PPC technique with different duty ratio, frequency and amplitude. The simulation results obtained from the PPC technique showed that the duty ratio and amplitude of the charging current are inversely proportional to the charging capacity. In the application of pulsed charging techniques, it is important to maintain the discharge capacity, charge capacity, charge time and cell temperature at nominal values. In the study carried out to investigate the effects of dynamic and static charging currents considering these criteria, it was observed that the dynamic fast charging profile after 1700 cycles has a significant role in reducing the charging time and capacity fade [22]. This study proposes a new pulsed charging technique to protect the aging and capacity loss of LIBs. Compared with other studies in the literature, the main contributions of this study are as follows:

- CC-CV and PPC techniques are explained in detail.
- With the proposed AHWPC technique, rest and charge transitions of the cell are performed more smoothly.

- CC-CV, PPC and AHWPC are compared in five different scenarios, different temperatures, different discharge currents and different DoDs.

This paper is organized as follows: in the second section, extensive information about the used LIBs charging techniques is given. In the third section, the implementation of the simulation methodology is explained in detail. The fourth section is devoted to the results and discussion, while the last section contains the conclusions of this study.

2. Battery Model and Charging Techniques

In this study, CC-CV mode, PPC mode and alternating half-wave current (AHWC) mode, which is proposed for the first time in this study, are used to determine aging, cell temperature and capacity losses in a $12.8V - 40Ah$ LIB model. The main focus of the study is to compare the performance of different charging techniques on the same cell. For this reason, the charging techniques were carried out on a battery model whose effectiveness has been proven by many studies [23,24].

2.1. CC-CV Mode

This charging technique consists of two stages, CC-mode and CV-mode. The first stage consists of CC-mode until the charging voltage provided by the manufacturer is reached. It must be ensured that the maximum charging current provided by the manufacturer is not exceeded during charging. The second phase, CV mode, consists of the time between the battery terminal voltage reaching the charging voltage and the charging current reducing to a limit value.

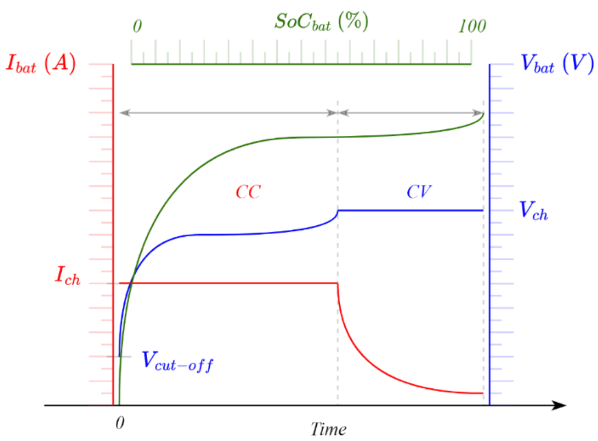

Figure 1: Variation of cell variables in CC-CV mode

Figure 1 represents the variation of cell voltage (V_{bat}), cell current (I_{bat}), and state of charge ratio (SoC_{bat}) of a fully discharged battery cell being fully charged by using CC-CV mode. In Figure 1, I_{ch} represents the battery charging current, V_{ch} represents the battery charging voltage, and $V_{cut-off}$ represents the discharge cut-off voltage. As can be seen, the battery cell, which was rapidly charging in CC-mode, shifted to CV-mode when the terminal voltage was equalized to the charging voltage. While the SoC curve changes rapidly in CC-mode, it changes very slowly in CV-mode. One of the biggest disadvantages of the CC-CV mode is that the CV-mode accounts for a significant portion of the charging time but a low portion of the discharge capacity. The relationship between SoC_{bat} and I_{ch} in Figure 1 can be given as follows:

$$SoC_{bat}(t) = SoC_{bat}(t-1) + \int_0^t \frac{I_{ch}}{Q_{bat}} dt \qquad (1)$$

In the notations in Equation 1, Q_{bat} is the rated battery capacity, and t is the time in seconds. Another disadvantage of using CC-CV mode in the charging protocol of LIBs is the growth of the SEI layer in the cell exposed to continuous charging current. This problem leads to capacity loss and therefore aging. The main causes of performance degradation in LIBs are loss of lithium inventory (LLI), loss of active material (LAM) and internal resistance which increases with time [25]. Among these reasons, it has been determined that LLI is the main cause of performance degradation [26]. Coulomb efficiency (CE) is usually used to determine the amount of LLI in a battery cell. CE is defined as follows:

$$\eta = \frac{C_d}{C_c} \qquad (2)$$

In Equation 2, η represents the Coulomb efficiency, C_d represents the discharge capacity in one cycle, and C_c represents the charge capacity in the same cycle.

2.2. PPC Mode

Positive Pulsed Current (PPC) mode consists of two phases within a certain period, namely the charging region and the relaxation region. In the charging region, a constant current is applied to the cell for a certain period of time, while this current is reduced to zero in the relaxation region. Figure 2a represents the implementation of the PPC technique. In this technique, a current source is connected to the battery via a switching element (S_t). By switching S_t periodically, pulsed charging currents are generated to charge the battery. Figure 2b shows the pulsed charging current waveforms. In the notations in Figure 2b, t_p represents the application time of the pulse currents, t_r the relaxation times of the battery cell, I_p is the amplitude of the applied pulse current, and T_p is the period of the pulse current. The relationship between the duty ratio (D_p), frequency (f_p), and T_p of the PPC is defined as follows:

$$f_p = \frac{1}{T_p} \tag{3}$$

$$D_p = \frac{t_p}{T_p} \tag{4}$$

When using the PPC mode, it should be noted that I_p does not exceed the maximum charging current, and t_r gives the battery cell sufficient relaxion time. In addition, for an objective comparison between the techniques, the average charging current in PPC mode must be equal to that in CC-CV mode. For example, a battery cell charged with 1C in CC-CV mode should be charged with 2C in PPC mode if D_p = %50. Research has shown that in addition to charging current, pulse frequency will also have a negative role in both fast charging and capacity fade. Among the pulse currents with the same amplitude and duty ratio at $50Hz$, $100Hz$, and $1kHz$, pulse currents at $50Hz$ and $1kHz$ showed more favorable results in terms of both fast charging and capacity losses compared to CC-CV mode. However, pulse currents of $100Hz$ result in both a significant increase in interfacial resistance and a decrease in interfacial capacity compared to CC-CV, which leads to an increase in SEI [27]. In addition, both experimental and simulation results have confirmed that it is possible to increase the cycle life of a battery cell by more than two times by using a suitable pulse current waveform [28]. Figure 3 shows the current, voltage and state of charge rate of a battery cell charged by PPC mode.

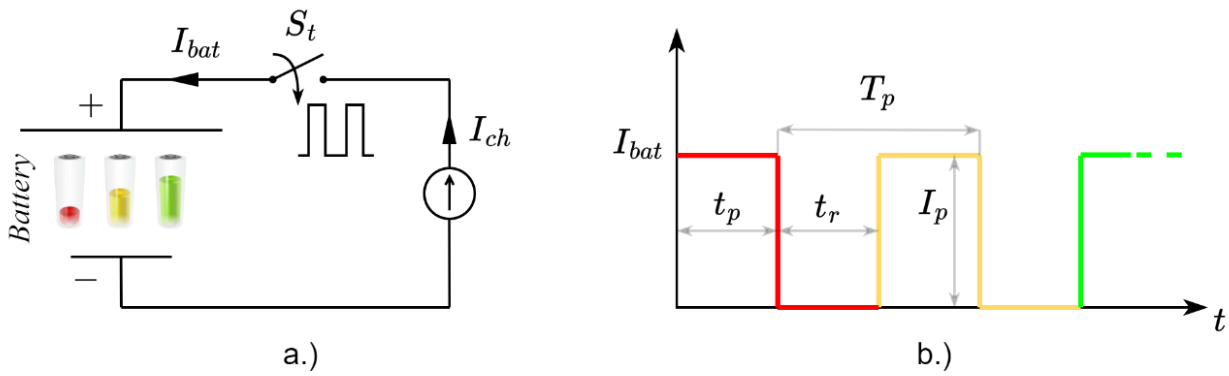

Figure 1: PPC mode a.) Equivalent circuit, b.) Pulsed current waveform

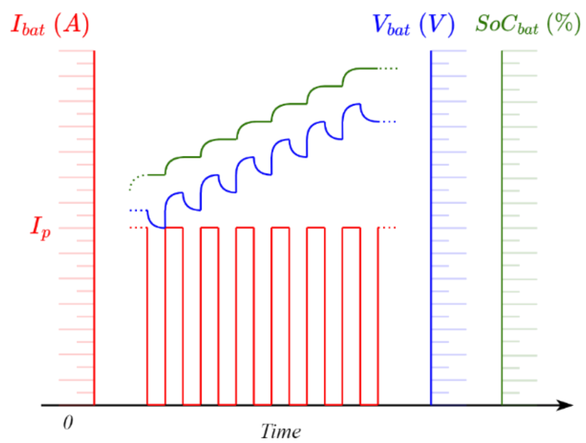

Figure 2: Variation of cell variables in PPC mode

The charging current I_p in Figure 3 is a pulsed current with an effective period of 50%. The average value of the pulsed current should not exceed the maximum charging current of the battery cell during a period. The pulse effects of the charging current are similarly observed on the cell voltage (V_{bat}) and the state of charge rate (SoC_{bat}). For highly efficient charging, pulse currents must be generated at maximum charging voltage. Each positive pulse results in a slight increase of V_{bat} and SoC_{bat}. As in CC-CV mode, the internal resistance of the cell plays an important role in all charging processes. If the internal resistance is high, a lower rise in the cell voltage is seen when the pulse current is applied, while when the pulse current is interrupted, the cell voltage will tend to drop rapidly due to the high internal resistance. This causes a longer charging time. Especially in the $SoC_{bat} < \%20$ and $SoC_{bat} > \%80$ ranges where the internal resistance is high [29] for each LIB cell, pulsed charging currents may be less effective than CC-CV mode. Another positive effect of PPC mode is that a certain rest time can be given to the battery cell in each period. This situation both reduces the LLI by preventing SEI growth and creates a natural commutation for the battery cell to cool down.

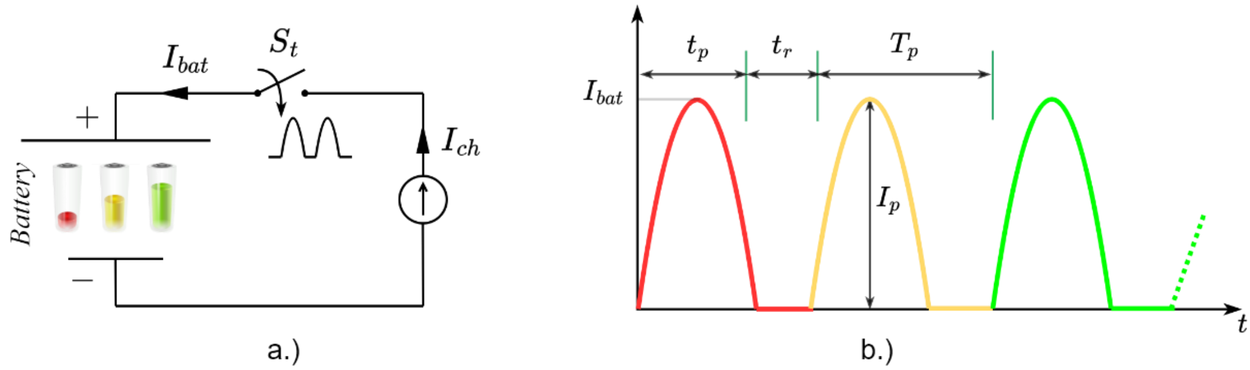

Figure 3: AHWPC mode a.) Equivalent circuit, b.) Alternating half wave pulsed current

2.3. Proposed AHWPC Mode

Alternating Half Wave Pulsed Current (AHWPC) mode is similar to PPC mode and consists of two stages, charging and resting regions. In the charging region, the charging current is applied to the cell as a sinusoidal half wave for a certain time (t_p). Then the cell is left to rest for a specific time (t_r). Figure 4 represents a battery cell charged by AHWPC mode. Figure 4a shows the electrical equivalent circuit of the AHWPC mode, and Figure 4b shows the pulse current waveform of the corresponding technique. This pulse current can be generated by using a half-wave rectifier circuit or a programmable DC power supply. When pulsed charging currents are applied, the average values of the applied charging current during t_p must be equal for all charging techniques. In this case, the average value expression of the pulsed current in Figure 4b can be written as follows:

$$I_{dc} = \frac{1}{T_p}\int_0^{T_p} I_{bat}\sin(wt)\,d(wt) \qquad (5)$$

In Equation 5, I_{dc} represents the average current value, and w represents the angular frequency. When the charging and relaxation regions of the pulse currents in Figure 4b are taken into account, Equation 5 can be rewritten as follows:

$$I_{dc} = \frac{1}{t_p + t_r}\int_0^{t_p} I_{bat}\,sin(wt)\,d(wt) \qquad (6)$$

Figure 5 compares the continuous CC-CV technique with the pulsed PPC and AHWPC techniques, highlighting their differences in current waveforms. In order to evaluate the charging techniques in terms of the aging and capacity fade, the areas $A_1 = A_2 = A_3$ must be equal. In Figure 5, A_{CC-CV}, A_{PPC}, and A_{AHWPC} represent the current amplitudes of CC-CV mode, PPC mode and AHWPC mode, respectively. For this study, $A_{CC-CV} = 0.5C$ is chosen. Therefore, the current applied to the battery cell for CC-CV mode during T_p can be expressed as follows:

$$I_{dc(CC-CV)} = 0.5C * T_p = A_1 \qquad (7)$$

In Equation 7, $I_{dc(CC-CV)}$ represents the average current value of the battery cell charged by CC-CV mode. In case the PPC technique is used, taking into account the relationship $A_1 = A_2$, the amplitude of the charging current in the PPC technique can be expressed as follows:

$$A_{PPC} * t_p = A_{CC-CV} * T_p = A_2 \qquad (8)$$

For $D = \%50$ duty ratio ($t_p = T_p/2$) in Equation 8, $A_{PPC} = 1C$ is obtained. With the use of the proposed AHWPC technique in the battery cell charging process and with the relationship $A_1 = A_3$ taken into account, the amplitude of the charging current can be expressed as follows:

$$\frac{A_{AHWPC}}{\pi} = A_{CC-CV} * T_p = A_3 \qquad (9)$$

In Equation 9, $A_{AHWPC} = 1{,}5708C$ value is obtained. The electrical properties of the battery cell used in the study are given in Table 1.

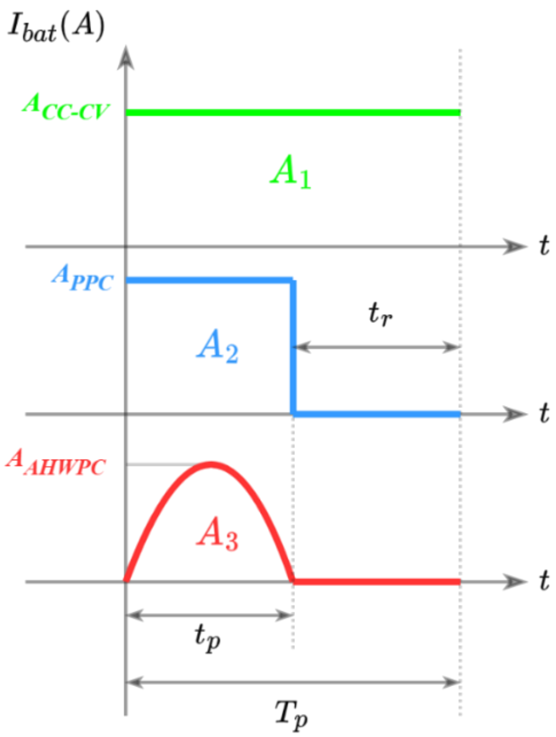

Figure 4: Continuous and pulsed charge current waveforms

Table 1: Electrical parameters of the battery cell

Parameter	Description	Value	Unit
R_{int}	Internal resistance	0.015	Ω
V_{nom}	Nominal voltage	12.8	V
C_{rated}	Rated capacity	40	Ah
$V_{cut-off}$	Cut-off voltage	10.5	V
V_{full}	Fully charged voltage	13.8	V
I_{d-nom}	Nominal discharge current	20	A

Thus, the amplitude of charging current in CC-CV technique is $A_{CC-CV} = 0{,}5C = 20A$, the amplitude of pulsed charging current in PPC technique is $A_{PPC} = 1C = 40A$ and the amplitude of sinusoidal pulsed charging current in AHWPC technique is $A_{AHWPC} = 1{,}5708C = 62{,}83A$.

3. Simulation Methodology

In order to compare the performances of CC-CV, PPC and the proposed AHWPC techniques described in detail in the previous section, the battery aging model available in MATLAB/SIMULINK environment is adopted as a reference.

In the simulation methodology used in this study, the battery cell was subjected to charge and discharge cycles at temperatures of $20°C$, $30°C$ and $40°C$ and at different depths of discharge (DoD) and different discharge rates for 1000 hours. The CC-CV mode simulation methodology for all temperature values is as follows:

$i.$) At $t = 0$, the battery cell with $SoC_{init} = \%100$ begins discharging with a rate of $0.5C$. Here, SoC_{init} represents the initial state of charge. The discharge process continues until $SoC = \%80$ ($DoD = \%20$). Then battery cell is charged at a rate of $0.5C$ until fully charged. This process is repeated for $200h$.

$ii.$) At $t = 200h$, the battery cell is discharged to $SoC = \%20$ and then fully charged again. This cycle is repeated for $200h$.

$iii.$) At $t = 400$, the methodology given in step one is applied again.

$iv.$) At $t = 600h$, the charge current is kept constant at $0.5C$ while the discharge current is increased to $2C$. This means that the battery will be charged with $0.5C$ and discharged with $2C$ in each cycle. These values are applied in the range $\%80 \leq SoC \leq \%100$.

$v.$) At $t = 800h$, the conditions in the first step are applied.

In PPC and AHWPC modes, DoD and discharge rates are applied similarly to the test procedure described above. However, positive and half sinusoidal pulse currents with 50% duty cycle at a frequency of $1Hz$ are applied to charge the battery cell. Figure 6 represents the application of the simulation methodology on the battery cell. In Figure 6, the programmable electronic load and the programmable DC power supply are connected to the battery cell via switches S_1 and S_2, respectively. Here, the programmable electronic load is used in the discharge process of the battery cell, and the programmable DC source is used in the charging process. Ratios of charging and discharging current (i_{ch}, i_{disch}), limit values of charging and discharging current (SoC_{min}, SoC_{max}), ambient temperature ($Ambient\ temp.$) are the data that must be provided externally for this methodology. Throughout the described methodology, the voltage, current, state of charge rate, temperature, aging and capacity values of the cell were measured. Since the charging and discharging processes will vary depending on the SoC when $SoC \leq SoC_{min}$, S_1 is turned on and S_2 is turned off to charge the battery cell with the selected charging rate and charging technique. Similarly, when $SoC \geq SoC_{max}$, S_1 is turned off and S_2 is turned on to discharge the battery cell with the selected discharge rate and DoD. For this study, $SoC_{min} = \%20$ in the fourth step of the test procedure and $SoC_{min} = \%80$ in the other steps. In all test procedures, $SoC_{max} = \%99$. More detailed information about the battery cell used in this study, aging and capacity measurements can be found in the following references [23,24,30]. Figure 7 illustrates the workflow of the simulation methodology.

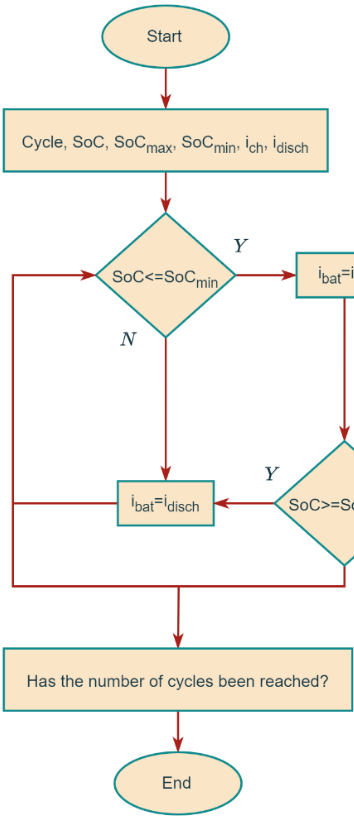

Figure 5: Flowchart of test methodology

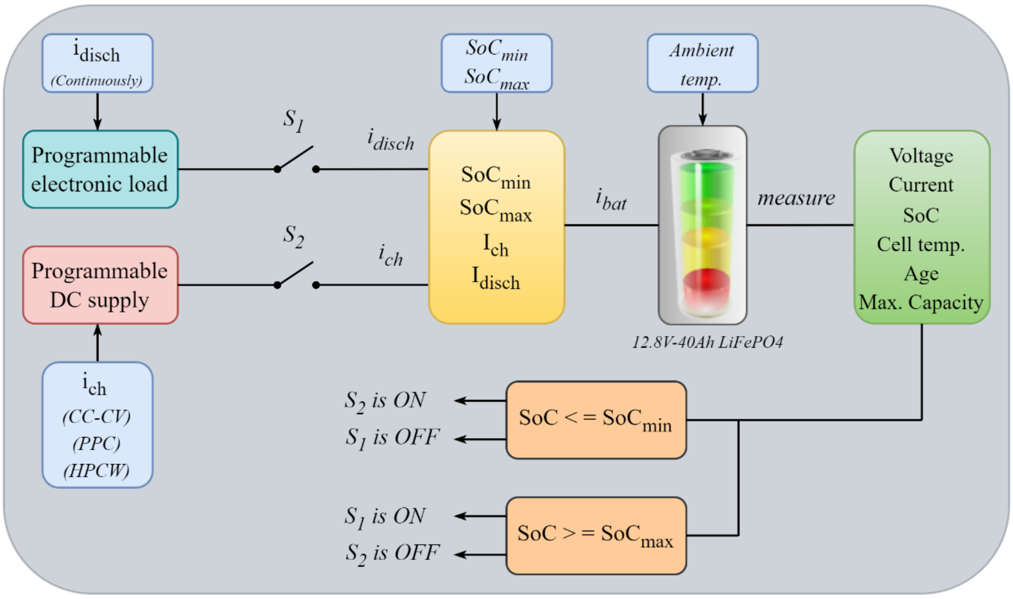

Figure 6: Demonstration of simulation methodology

4. Results and Discussion

Since the main framework of this study is to investigate the effects of pulsed charging currents on cell aging and capacity loss, the discharge currents are the same and continuous for all charging techniques. Five different cases were performed in each cycle as described in the test procedure. In addition, the effect of pulsed charging profiles at different temperatures was also investigated. The current profiles used for all temperature values are shown in Figure 8. The regions marked with the numbers i, ii, iii, iv, and v in Figure 8a represent the steps of the test procedure, respectively. In each of these regions, the specified charging and discharging techniques were applied to the cell for $200h$. As can be seen, the discharge current is the same for all cycles except for region ($i_{disch} = 20A = 0.5C$). In order to show the effect of cell aging, capacity loss and cell temperature at high currents, the discharge current was increased to $i_{disch} = 80A = 2C$ in region iv. The frequency of the pulsed charging currents during the whole cycle was chosen as $f_{i_{ch}} = 1\,Hz$. Although this value is frequently used in previous studies, further analysis on frequency optimization can improve the performance of pulsed charging techniques. Figure 8b represents a zoom-in view of the charging and discharging profiles applied to the battery cell over the whole cycle for a given period. It can be seen that the charging current, which is $0.5C$ in the CC-CV technique, is $1C$ and $1.5708C$ in the PPC and AHWPC techniques, respectively. As in the current profiles, it was observed that the cell voltages and state of charge were similar for all temperature values throughout the cycle.

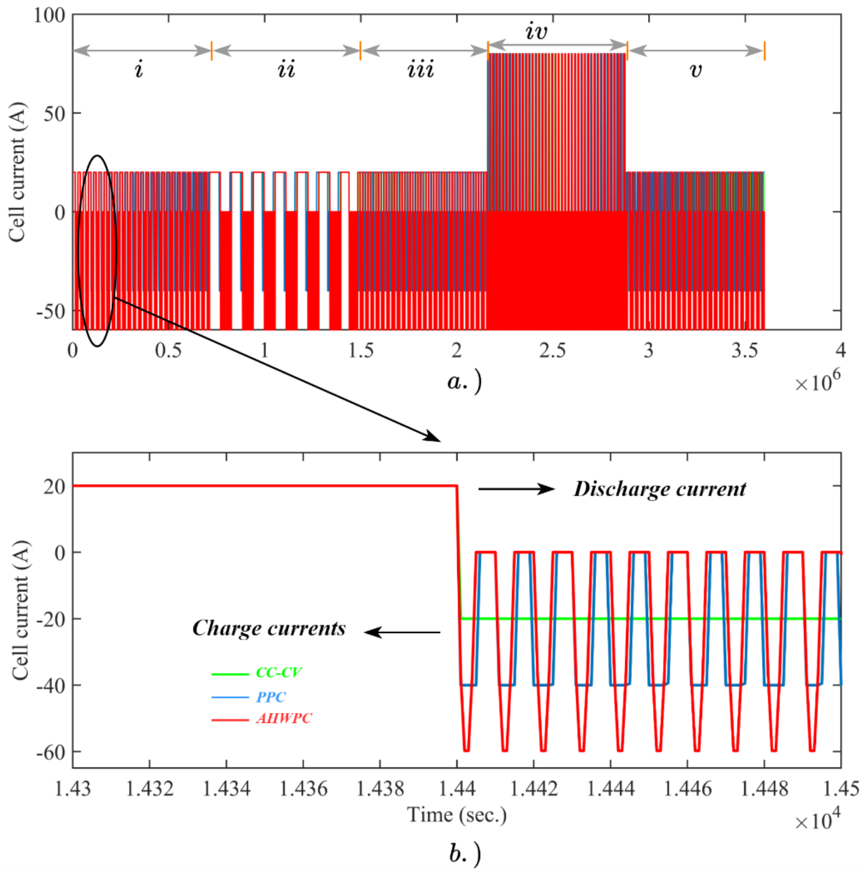

Figure 7: Continuous and pulsed current profiles used in the test procedure

Figure 9a and Figure 9b show the change in cell voltage and SoC, respectively. Due to the long cycle time, zoomed views are also shown at the bottom of the relevant images for a certain period of time to observe the changes clearly. The cell voltage in Figure 9a varies between approximately $13.2V$ and $15.8V$ in the first region. In the second region, by increasing $DoD = \%80$, the cell voltage begins to change more slowly between $12.5V$ and $14.8V$. This is an expected result as the DoD is increased. In the zoomed image in Figure 9a, the change of the cell voltage is similar to the change of the current profile. It can be concluded that this is due to the effect of the internal resistance (IR) of the cell changing at very small intervals. A similar result to the first region was observed in the third and fifth regions. In the fourth region, the cell voltage changed between $12.3V$ and $14.7V$ as the DoD increased to $2C$. When the SoC curves in Figure 9b are examined, it can be observed that the effect of all pulsed charging techniques on SoC is similar. Therefore, the similar changes in cell voltages and SoCs of CC-CV, PPC and the AHWPC techniques show the applicability of the proposed technique. Aging, capacity fade and temperature of the battery charged with the mentioned techniques when the ambient temperature is $20°C$ are shown in Figures 10a, 10b and 10c, respectively. Cell aging in Figure 10a equivalently corresponds to one cycle. Therefore, the battery cell charged with the CC-CV technique completed a full cycle of approximately 16.5145 times at the end of the cycle. It should be noted that a cycle occurs when a fully charged battery cell is first fully discharged and then fully charged again. In the first region (i), all charging techniques exhibit a similar ageing profile. In this region, the CC-CV mode aging factor was measured as 2.321. PPC and AHWPC techniques have an ageing value corresponding to 1.343 cycles in the same region. In the second region (ii), the increase in the aging rate is clearly seen by increasing the DoD to 80%. The aging factors at the end of this region are 6.343 in CC-CV mode and approximately 3.512 in PPC and AHWPC modes. In the third region (iii), it is seen that the aging rate decreases in all charging methods by decreasing the DoD to 20%. At the end of this cycle, the aging in the battery cell was observed to be approximately 8.968, 4.858 and 4.928 in CC-CV, PPC and AHWPC modes, respectively. In the fourth region (iv), the aging values were measured as 14.075, 7.741 and 7.576 in CC-CV, PPC and AHWPC techniques, respectively, as a result of the increase in the aging rate with increasing the discharge current to $2C$. In the fifth region (v), the aging rate decreased when the discharge current was reduced to $0.5C$. At the end of this region, the aging values were observed as 16.514 in CC-CV, 9.063 in PPC, and 8.929 in AHWPC.

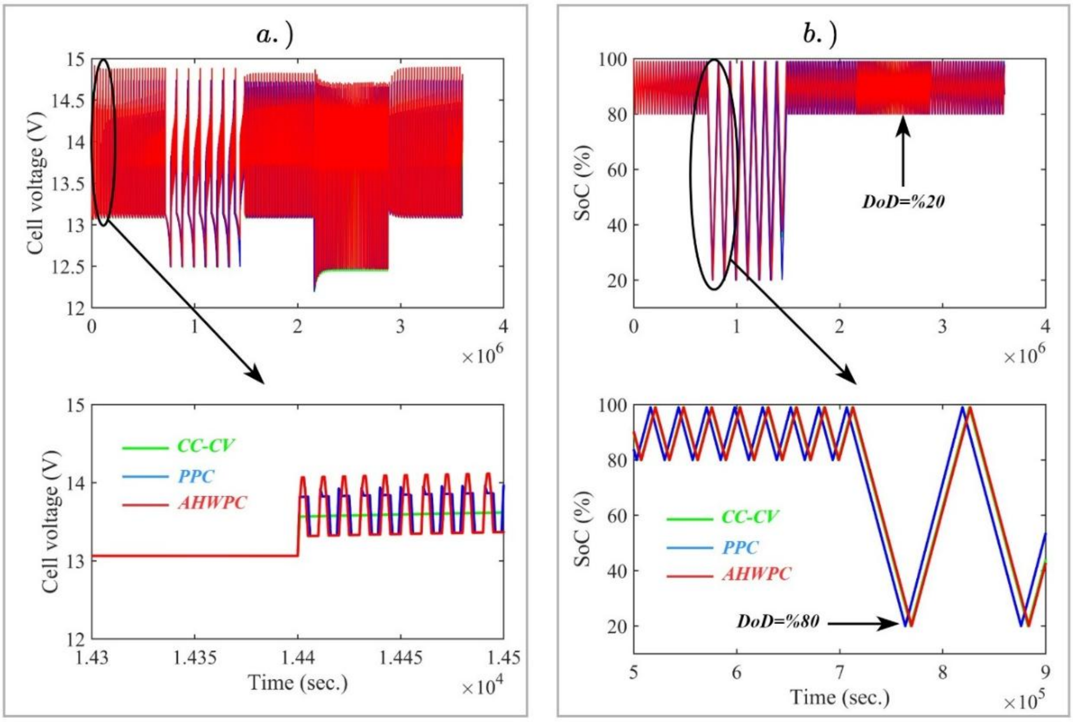

Figure 8: During the test procedure a.) Cell voltage, b.) SoC

Figure 10b represents the capacity losses in the battery cells during the test. It is seen that capacity fade increases rapidly in the regions where aging accelerates. At the end of the simulation, the capacity fades in the battery cell charged by CC-CV, PPC, and AHWPC methods were measured as 0.1826%, 0.1003%, and 0.0987%, respectively. In terms of capacity loss, it can be said that the PPC technique is superior to AHWPC in the second and third regions. In the first region, it can be stated that the capacity loss for both techniques is similar. However, in the fourth and fifth regions, the AHWPC technique outperformed PPC. The AHWPC technique will increase this superiority further if the charge and discharge cycles continue. Figure 10c shows the temperature change of the battery cell as a result of applying the relevant charging techniques to the battery cell at $20°C$ ambient temperature. In the first, second, and third regions, the cell temperature increased by approximately 35%. It is seen that the charging techniques have no significant effect on the cell temperature. However, by increasing the discharge current from $0.5C$ to $2C$ (region v), the cell temperature increased from $27°C$ to $37°C$. In addition, changing the DoD did not cause a significant change in battery cell temperature. The aging, capacity loss, and temperature of the battery charged by the aforementioned techniques at the ambient temperature of $30°C$ are shown in Figures 11a, 11b, and 11c, respectively. In the aging curves in Figure 11a, it is seen that aging is similar for all three techniques in the first region. In this region, the full cycle equivalent aging values were measured as 2.836, 1.596, and 1.645 for CC-CV, PPC, and AHWPC techniques, respectively. In the first region, the PPC technique outperformed the other two techniques. At the end of the second region, the aging effect, which was 8.376 in the CC-CV technique, and 4.539 in the PPC and the AHWPC techniques. At the end of the third region, similar to the second region, the aging rate increased in CC-CV while it was lower in PPC and AHWPC techniques. The proposed AHWPC mode is superior to the other two methods in the fourth and fifth regions. The aging values at the end of the cycle were 20.244 for CC-CV, 11.175 for PPC, and 10.816 for AHWPC. The capacity curves in Figure 11b show that the capacity loss in PPC and AHWPC techniques in the first, second, and third regions are similar, and they perform better than the CC-CV technique.

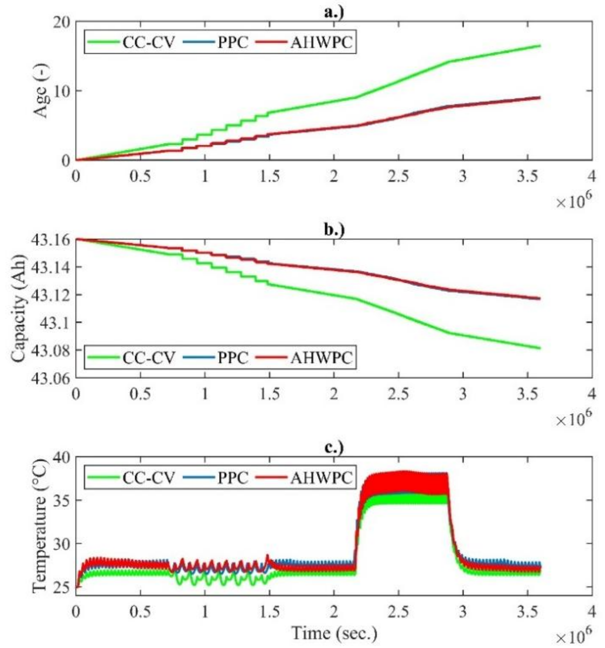

Figure 9: Simulation results, a.) Age, b.) Capacity fade, c.) Cell temperature (20 °C)

The proposed AHWPC technique was outstanding compared to the other methods in the fourth and fifth regions. In the fourth region, the maximum capacities were observed at 43.063 for CC-CV, 43.106 for PPC, and 43.108 for AHWPC.

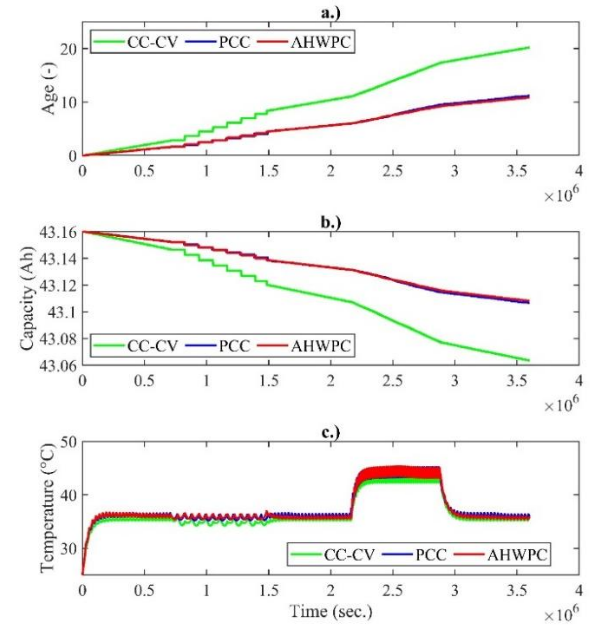

Figure 10: Simulation results, a.) Age, b.) Capacity fade, c.) Cell temperature (30 °C)

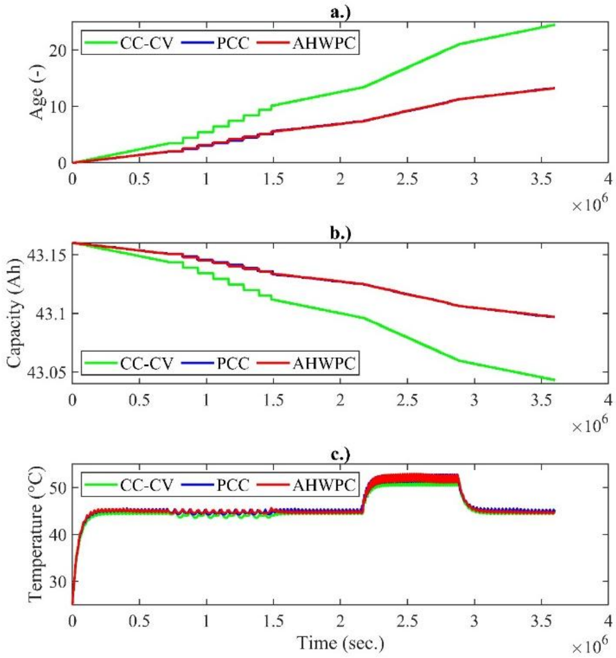

Figure 11: Simulation results, a.) Age, b.) Capacity fade, c.) Cell temperature (40 °C)

The capacity losses at the end of the cycle were calculated at 0.2238% for CC-CV, 0.1235% for PPC, and 0.1196% for AHWPC. In the cell temperature curves in Figure 11c, it is approximately $36°C$ in the first, second, and third regions. In this case, cell temperatures have increased by approximately 20%. However, it can be said that CC-CV performs better in terms of cell temperature, although at a low level. The aging, capacity loss, and temperature of the battery charged with the abovementioned techniques at $40°C$ ambient temperature is shown in Figures 12a, 12b, and 12c, respectively. When the aging curves in Figure 12a are examined, PPC and AHWPC exhibited similar results throughout the test procedure. In CC-CV, the aging rate increased even more with the increase in temperature. At the end of the simulation cycle, the equivalent full-cycle aging values were measured as 24.519 for CC-CV, 13.231 for PPC, and 13.167 for AHWPC. When the capacity losses in Figure 12b are evaluated, it is seen that PPC and AHWPC techniques outperform CC-CV. While the capacity loss in CC-CV is approximately 0.2711%, this value is 0.1464% in PPC and 0.1457% in AHWPC. In the cell temperature variations in Figure 12c, it can be said that the charging techniques yield similar results.

Table 2 summarizes the aging and maximum capacity retention of the battery under different charging techniques and temperatures. The lowest aging and highest capacity retention values, marked in bold, indicate the superior performance of AHWPC. As can be seen, the proposed AHPWC technique exhibited superior results compared to the other two methods in both maintaining the maximum capacity and delaying the aging effect. The aging curves of the charging techniques for different temperature values used in the simulation procedure are shown in Figure 13.

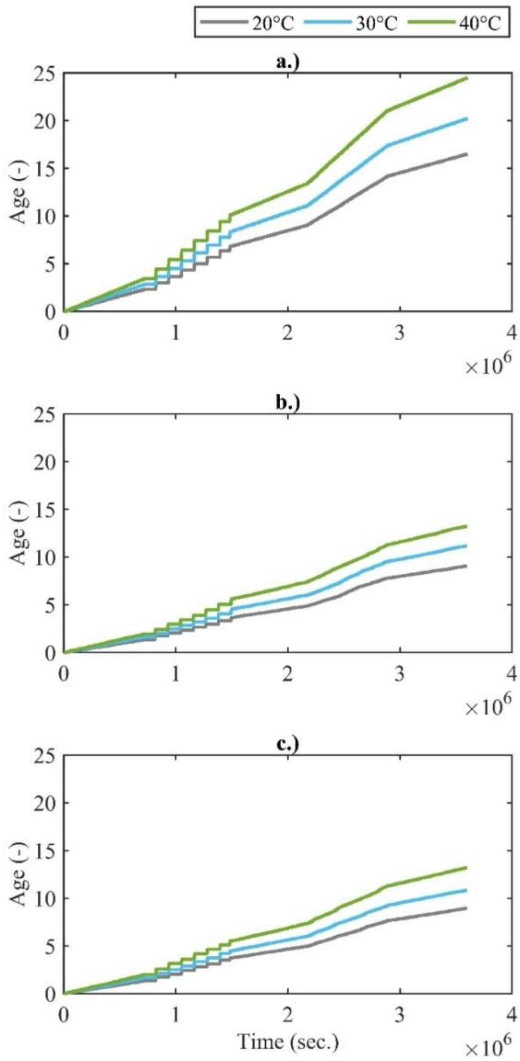

Figure 12: The aging effect of the battery cell at different temperatures a.) CC-CV, b.) PPC, c.) AHWPC

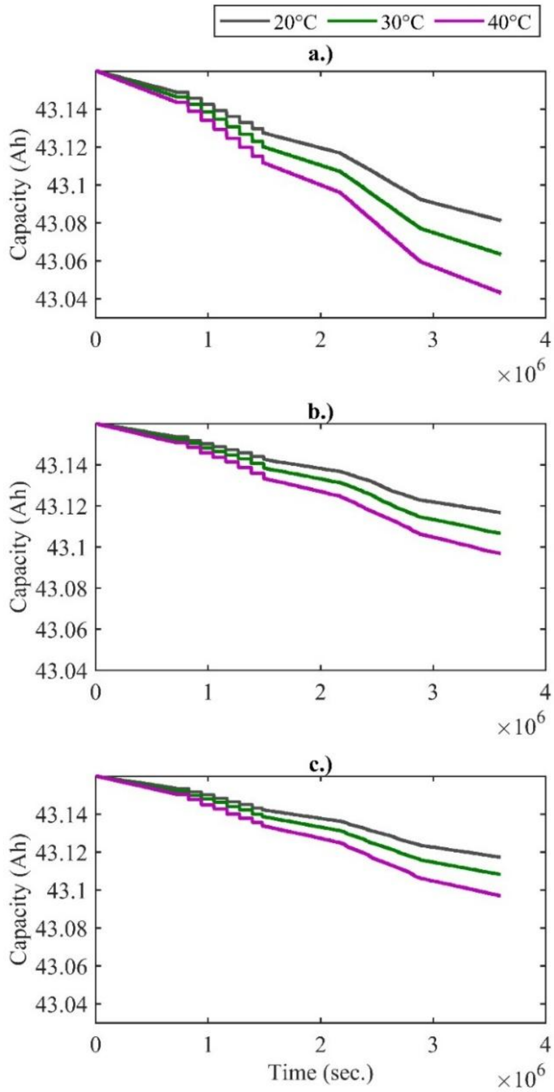

Figure 13: The capacity fades of the battery cell at different temperatures a.) CC-CV, b.) PPC, c.) AHWPC

These curves can also be obtained separately from the previous results. However, to demonstrate the superiority of the proposed AHWPC technique over PPC and CC-CV techniques, it is thought that comparing the performances of the same charging technique under different temperature values will emphasize the importance of the study. Figures 13a, 13b, and 13c show the aging performances of CC-CV, PPC, and AHWPC charging techniques at $20°C$, $30°C$, and $40°C$ ambient temperatures, respectively. As a result of completing the test cycle at $20°C$ ambient temperature with the CC-CV technique, the aging value of the battery cell corresponded to a cycle number of approximately 16.514.

By increasing the ambient temperature to $30°C$, this value increased by 18.425% compared to $20°C$. In the same technique, this rate increased to 32.648% when increasing the ambient temperature to $40°C$. According to the aging curves of the PPC technique in Figure 13b, the aging value at $20°C$ ambient temperature was measured to be equivalent to 9.063 cycles. By increasing the ambient temperature to $30°C$, the aging value increased by 18.899%. In the same technique, this rate increased to 31.501% when increasing the ambient temperature to $40°C$. When the aging curves of the AHWPC technique in Figure

13c are evaluated, the aging value at $20°C$ was measured as 8.929.

The aging value increased by 17.446% in the same technique at $30°C$ ambient temperature, and this rate increased to 32.186% at $40°C$ ambient temperature. Figure 14 shows the maximum capacity curves of the battery cell charged by CC-CV, PPC, and AHWPC techniques at different ambient temperatures. According to the results obtained by using the CC-CV technique in Figure 14a, the maximum capacity values were measured as 43.081, 43.063, and 43.043 at $20°C$, $30°C$ and $40°C$ ambient temperatures, respectively. These values are observed as 43.116, 43.106, and 43.096 in the curves of the PPC technique in Figure 14b, respectively. The results of the AHWPC technique in Figure 14c showed that the maximum capacities were 43.117 at $20°C$, 43.108 at $30°C$, and 43.097 at $40°C$. Since the numerical results in Table 2 are pretty close, comparing charging techniques may not be easy. Figure 15 compares the numerical results obtained from this study more clearly.

Table 2: Numerical test results

	Temperature (°C)					
	20		30		40	
	Age	Capacity	Age	Capacity	Age	Capacity
$CC-CV$	16.5145	43.0812	20.2448	43.0634	24.5196	43.0430
PPC	9.06535	43.1167	11.1754	43.1067	13.2316	43.0968
$AHWPC$	**8.92912**	**43.1174**	**10.8163**	**43.1084**	**13.1675**	**43.0971**

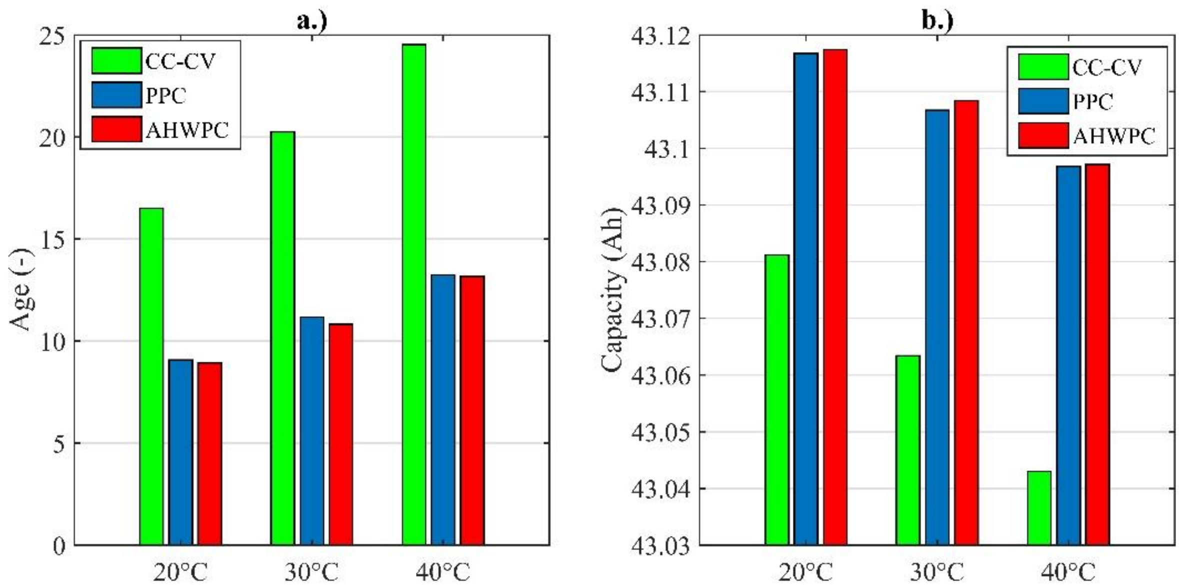

Figure 14: Effects of charging techniques at different temperatures a.) Age, b.) Maximum capacity

Figure 15a compares aging values for all charging techniques at the temperature values selected for this study. As seen, aging increases as temperature increases for all three techniques. However, it can be said that the CC-CV technique is more sensitive to temperature, and the aging rate rises more than that of the other two techniques as the temperature increases. Figure 15b represents a visualization of the capacity results obtained by using the relevant charging techniques at selected ambient temperatures. As the ambient temperature increases, the capacity loss in the CC-CV technique increases faster than the other two techniques. Pulsed charging techniques reduce heat accumulation compared to CC-CV mode by preventing continuous high current flow. This reduction in thermal stress is expected to slow down

SEI layer growth, potentially extending battery lifespan. For all three temperature values, the AHWPC technique performed better than the CC-CV and PPC techniques. Continuous charging currents in battery cells cause more thermal runaway. It is also known that suddenly changing the charging current causes more aging. Therefore, the superior performance of the AHWPC technique can be attributed to the smoother rise and fall of the charging current.

5. Conclusion

This paper presents a new pulsed charging technique for reducing aging and capacity losses in LIBs. The proposed AHWPC technique is compared with the CC-CV technique, which is widely used in existing studies, and the PPC technique, which was introduced in recent years to improve fast charging techniques. The three charging techniques mentioned above are compared regarding aging, capacity losses, and cell temperatures on a $12V-40Ah$ lithium-ion battery. When the results obtained are evaluated together, it is seen that the CC-CV technique shows superior performance only at the cell temperature during the test cycle and is considerably weaker than the other two techniques in terms of aging and capacity fade. Also, it was observed that with increasing ambient temperature, the aging rate and capacity fade in the CC-CV technique increased more than the other two techniques. Although the PPC and the AHWPC techniques had similar aging and capacity fade values throughout the cycle, the AHWPC technique outperformed the PPC technique at all temperature values. At $20°C$, aging in PPC was reduced by approximately 45% compared to CC-CV. AHWPC technique provided a 2% improvement in aging compared to PPC. At $30°C$, PPC reduced cell aging by 44.79% compared to CC-CV, while AHWPC completed the test procedure with 3.21% less aging than PPC. At $40°C$, the PPC technique provided 46.03% superiority over CC-CV, while the AHWPC technique achieved approximately 0.5% lower aging performance than PPC. This result is attributed to the lower LAM and LLI loss in the AHWPC technique due to the smoother change of charging currents. As a result, the AHWPC technique is considered to be a serious competitor to existing charging techniques. The selection of $1\,Hz$ pulse frequency for pulse charging techniques is a limitation of this study. In future studies, the performance of pulse charging currents with different pulse frequencies and duty ratios on aging and capacity losses will be evaluated.

Article Information

Financial Disclosure: The author (s) has not received any financial support for the research, authorship or publication of this study.

Authors' Contrtibution: Concept, Design, Supervision, Resources, Data Collection, Analysis, Literature Search, Writing Manuscript, Critical Review: **Muhammed Reşit ÇORAPSIZ**

Conflict of Interest/Common Interest: No conflict of interest or common interest has been declared by the authors.

Ethics Committee Approval: This study does not require ethics committee permission or any special permission.

References

[1] Amanor-Boadu J. M., Guiseppi-Elie A., Sánchez-Sinencio E., The Impact of Pulse Charging Parameters on the Life Cycle of Lithium-Ion Polymer Batteries, Energies, 11 (8), 2162, 2018.

[2] Lithium-ion Battery Market. https://www.precedenceresearch.com/lithium-ion-battery-market#:~:text=The%20Asia%20Pacific%20lithium%2Dion,with%20revenue%20share%20of%2047%25.

[3] Su X., Xu X.-P., Ji Z.-Q., Wu J., Ma F., Fan L.-Z., Polyethylene Oxide-Based Composite Solid Electrolytes for Lithium Batteries: Current Progress, Low-Temperature and High-Voltage Limitations, and Prospects, Electrochemical Energy Reviews, 7 (1), 2, 2024.

[4] Gielinger S., Hein T., Ziegler A., Oeser D., Breitfelder S., Bohn G., A Short Time Expansion Measurement Method for the Detection of Aging Effect of Lithium Ion Cells Using a High Resolution Laser Interfometric Setup, IEEE Access, 11, 139924-139934, 2023.

[5] Diolaiti V., Andreoli A., Chauque S., Bernardoni P., Mangherini G., Ricci M., Zaccaria R. P., Ferroni M., Vincenzi D., Comparison of Porous Germanium Thin Films on SS and Mo as Anode for High-Performance LIBs, IEEE Transactions on Nanotechnology, 22, 552-557, 2023.

[6] Huang X., Liu W., Meng J., Li Y., Jin S., Teodorescu R., Stroe D. I., Lifetime Extension of Lithium-Ion Batteries With Low-Frequency Pulsed Current Charging, IEEE Journal of Emerging and Selected Topics in Power Electronics, 11 (1), 57-66, 2023.

[7] Huang X., Meng J., Liu W., Ru F., Duan C., Xu X., Stroe D. I., Teodorescu R., Lithium-Ion Battery Lifetime Extension With Positive Pulsed Current Charging, IEEE Transactions on Industrial Electronics, 71 (1), 484-492, 2024.

[8] Yan H. W., Farivar G. G., Beniwal N., Tafti H. D., Ceballos S., Pou J., Konstantinou G., Battery Lifetime Extension in a Stand-Alone Microgrid With Flexible Power Point Tracking of Photovoltaic System, IEEE Journal of Emerging and Selected Topics in Power Electronics, 11 (2), 2281-2290, 2023.

[9] Lv H., Huang X., Liu Y., Analysis on pulse charging–discharging strategies for improving capacity retention rates of lithium-ion batteries, Ionics, 26 (4), 1749-1770, 2020.

[10] Chen P.-T., Yang F.-H., Cao Z.-T., Jhang J.-M., Gao H.-M., Yang M.-H., Huang K. D., Reviving Aged Lithium-Ion Batteries and Prolonging their Cycle Life by Sinusoidal Waveform Charging Strategy, Batteries & Supercaps, 2 (8), 673-677, 2019.

[11] Li H., Zhang X., Peng J., He J., Huang Z., Wang J., Cooperative CC–CV Charging of Supercapacitors Using Multicharger Systems, IEEE Transactions on Industrial Electronics, 67 (12), 10497-10508, 2020.

[12] Lee Y. D., Park S. Y., Electrochemical State-Based Sinusoidal Ripple Current Charging Control, IEEE Transactions on Power Electronics, 30 (8), 4232-4243, 2015.

[13] Zhu S., Hu C., Xu Y., Jin Y., Shui J., Performance improvement of lithium-ion battery by pulse current, Journal of Energy Chemistry, 46, 208-214, 2020.

[14] Huang X., Li Y., Acharya A. B., Sui X., Meng J., Teodorescu R., Stroe D.-I., A Review of Pulsed Current Technique for Lithium-ion Batteries, Energies, 13 (10), 2458, 2020.

[15] Tang A., Gong P., Huang Y., Wu X., Yu Q., Research on pulse charging current of lithium-ion batteries for electric vehicles in low-temperature environment, Energy Reports, 9, 1447-1457, 2023.

[16] Chen L. R., Wu S. L., Shieh D. T., Chen T. R., Sinusoidal-Ripple-Current Charging Strategy and Optimal Charging Frequency Study for Li-Ion Batteries, IEEE Transactions on Industrial Electronics, 60 (1), 88-97, 2013.

[17] Li J., Murphy E., Winnick J., Kohl P. A., The effects of pulse charging on cycling characteristics of commercial lithium-ion batteries, Journal of Power Sources, 102 (1), 302-309, 2001.

[18] MOLICEL Lithium-ion Rechargeable Battery Cell Characteristics. https://www.molicel.com/wp-content/uploads/INR18650M35A-V2-80096.pdf. 29.02.2024.

[19] ORION 18650P/25 Lithium Ion Cell. https://static.ticimax.cloud/37661/uploads/dosyalar/orion-18650p-2500.pdf. 29.02.2024.

[20] Keil P., Jossen A., Charging protocols for lithium-ion batteries and their impact on cycle life—An experimental study with different 18650 high-power cells, Journal of Energy Storage, 6, 125-141, 2016.

[21] Savoye F., Venet P., Millet M., Groot J., Impact of Periodic Current Pulses on Li-Ion Battery Performance, IEEE Transactions on Industrial Electronics, 59 (9), 3481-3488, 2012.

[22] Abdel-Monem M., Trad K., Omar N., Hegazy O., Van den Bossche P., Van Mierlo J., Influence analysis of static and dynamic fast-charging current profiles on ageing performance of commercial lithium-ion batteries, Energy, 120, 179-191, 2017.

[23] Tremblay O., Dessaint L. A., Dekkiche A. I., A Generic Battery Model for the Dynamic Simulation of Hybrid Electric Vehicles, 2007 IEEE Vehicle Power and Propulsion Conference, 284-289, 9-12 Sept. 2007.

[24] Omar N., Monem M. A., Firouz Y., Salminen J., Smekens J., Hegazy O., Gaulous H., Mulder G., Van den Bossche P., Coosemans T., Van Mierlo

J., Lithium iron phosphate based battery – Assessment of the aging parameters and development of cycle life model, Applied Energy, 113, 1575-1585, 2014.

[25] Yang F., Wang D., Zhao Y., Tsui K.-L., Bae S. J., A study of the relationship between coulombic efficiency and capacity degradation of commercial lithium-ion batteries, Energy, 145, 486-495, 2018.

[26] Dubarry M., Liaw B. Y., Identify capacity fading mechanism in a commercial LiFePO4 cell, Journal of Power Sources, 194 (1), 541-549, 2009.

[27] Rajagopalan Kannan D. R., Weatherspoon M. H., The effect of pulse charging on commercial lithium nickel cobalt oxide (NMC) cathode lithium-ion batteries, Journal of Power Sources, 479, 229085, 2020.

[28] Li Q., Tan S., Li L., Lu Y., He Y., Understanding the molecular mechanism of pulse current charging for stable lithium-metal batteries, Science Advances, 3 (7), e1701246, 2017.

[29] Kopczyński A., Liu Z., Krawczyk P., Parametric analysis of Li-ion battery based on laboratory tests, E3S Web Conf., 44, 00074, 2018.

[30] 12.8 V, 40 Ah, Lithium-Ion (LiFePO4) Battery Aging Model (1000 h Simulation). https://www.mathworks.com/help/sps/ug/12-8-v-40-ah-lithium-ion-lifepo4-battery-aging-model-1000-h-simulation.html. 17.03.2024.